OPEN

Citation: Cell Death and Disease (2013) 4, e915; doi:10.1038/cddis.2013.442

www.nature.com/cddis

An EMT spectrum defines an anoikis-resistant and spheroidogenic intermediate mesenchymal state that is sensitive to e-cadherin restoration by a src-kinase inhibitor, saracatinib (AZD0530)

RY-J Huang*[,1,2], MK Wong[2], TZ Tan[2], KT Kuay[2], AH C Ng[6], VY Chung[2], Y-S Chu[6], N Matsumura[4], H-C Lai[5], YF Lee[2], W-J Sim[6], C Chai[2], E Pietschmann[1], S Mori[2,3], JJ H Low[1], M Choolani[1] and JP Thiery*[,2,6,7]

The phenotypic transformation of well-differentiated epithelial carcinoma into a mesenchymal-like state provides cancer cells with the ability to disseminate locally and to metastasise. Different degrees of epithelial–mesenchymal transition (EMT) have been found to occur in carcinomas from breast, colon and ovarian carcinoma (OC), among others. Numerous studies have focused on *bona fide* epithelial and mesenchymal states but rarely on intermediate states. In this study, we describe a model system for appraising the spectrum of EMT using 43 well-characterised OC cell lines. Phenotypic EMT characterisation reveals four subgroups: Epithelial, Intermediate E, Intermediate M and Mesenchymal, which represent different epithelial–mesenchymal compositions along the EMT spectrum. In cell-based EMT-related functional studies, OC cells harbouring an Intermediate M phenotype are characterised by high N-cadherin and *ZEB1* expression and low E-cadherin and *ERBB3*/HER3 expression and are more anoikis-resistant and spheroidogenic. A specific Src-kinase inhibitor, Saracatinib (AZD0530), restores E-cadherin expression in Intermediate M cells in *in vitro* and *in vivo* models and abrogates spheroidogenesis. We show how a 33-gene EMT Signature can sub-classify an OC cohort into four EMT States correlating with progression-free survival (PFS). We conclude that the characterisation of intermediate EMT states provides a new approach to better define EMT. The concept of the EMT Spectrum allows the utilisation of EMT genes as predictive markers and the design and application of therapeutic targets for reversing EMT in a selective subgroup of patients.

Cell Death and Disease (2013) **4,** e915; doi:10.1038/cddis.2013.442; published online 7 November 2013
Subject Category: Cancer

Epithelial–mesenchymal transition (EMT), a fundamental mechanism in embryonic development, is crucial in carcinoma progression.[1] The EMT programme contributes to the dissemination of carcinoma cells from solid tumours and the formation of micro-metastatic foci that subsequently develop into clinically detectable metastases.[2] EMT describes a process that controls the progressive loss of epithelial characteristics and the acquisition of mesenchymal features,[3] as well as the acquisition of chemoresistance,[4] immune escape[5] and the maintenance of cancer stemness.[6,7] Fluctuations in several molecular markers are commonly used to assess the EMT status, such as an increase in the mesenchymal marker, vimentin and/or a decrease in the epithelial markers, E-cadherin and cytokeratin.[1,3] However, studies usually overlook the progressive changes during intermediate cellular states.[8,9] An intermediate state implies a spectrum of heterogeneity for EMT (rather than two extreme ends of the process), with potentially metastable, plastic intermediate cells. Indeed, cells within intermediate states express traits of a mixed lineage, with double positivity of cytokeratins and vimentin.[8] However, few studies have addressed the functionality of these transitory states, an oversight partly caused by the lack of a detailed understanding of EMT and the current dearth of reliable readouts for its progression. Thus, the existence of intermediate states, which may also occur during carcinoma progression,[10] has not been well appreciated.

Cancer cell line collections, such as the US National Cancer Institute (NCI) 60 human tumour cell line (NCI60), serve as models for drug discovery,[11] and as robust tools for modelling

[1]Department of Obstetrics & Gynaecology, National University Hospital, Singapore 119228, Singapore; [2]Cancer Science Institute of Singapore, National University of Singapore, Singapore 117599; [3]Division of Cancer Genomics, Cancer Institute of Japanese Foundation for Cancer Research, 3-8-31 Ariake, Koto-ku, Tokyo 135-8550, Japan; [4]Department of Obstetrics and Gynecology, Kyoto University, Kyoto 606-8507, Japan; [5]Department of Obstetrics and Gynecology, National Defense Medical Center, Tri-Service General Hospital, Taipei, Taiwan; [6]Institute of Molecular and Cell Biology, A*STAR, Singapore 138673, Singapore and [7]Department of Biochemistry, National University of Singapore, Singapore 117597, Singapore
*Corresponding author: RY-J Huang, CSI Singapore, NUS Centre for Translational Medicine NUS Yong Loo Lin School of Medicine, 14 Medical Drive, Singapore 117599, Singapore. Tel: +65 6516 1148; Fax: +65 6779 4753; E-mail: ruby_yj_huang@nuhs.edu.sg
or JP Thiery, Institute of Molecular and Cell Biology, A;STAR, Singapore 138673, Singapore. Tel: +65 6516 3241/42; Fax: +65 6779 1453; E-mail: jpthiery@imcb.a-star.edu.sg
Keywords: epithelial–mesenchymal transition; intermediate states; ovarian cancer
Abbreviations: EMT, Epithelial–mesenchymal transition; NCI, National Cancer Institute; ECM, Extracellular matrix; OC, Ovarian carcinoma; MET, Mesenchymal–epithelial transition; Intermediate E, Intermediate epithelial; Intermediate M, Intermediate mesenchymal; QPCR, Quantitative PCR; VI, Viability index; ULAS, Ultra-low attachment suspensions; TCP, Tissue culture plastic; PFS, Progression-free survival; RMST, Restricted mean survival time; GSEA, Gene-set enrichment analysis
Received 24.7.13; revised 03.10.13; accepted 04.10.13; Edited by G Raschellá

in vivo tumours. Indeed, breast and ovarian cancer cell line collections, for example, have retained molecular characteristics corresponding to those of their *in vivo* counterparts, thus providing powerful options for modelling cancer heterogeneity *in vitro*[12,13] and for studying the several hallmarks of cancer.[14] However, EMT phenotyping in these *in vitro* models has not been systematically explored. One protocol proposes the use of morphological and molecular features to indicate EMT status, including the loss of cell–cell contact, elongation of cell shape, increased scattering migration/invasion and resistance to anoikis.[15] Other *in vitro* studies have also demonstrated the importance of characterising EMT phenotypes in cancer cell lines[16–18] to provide insight into the biological relevance of the EMT status.

Anoikis describes apoptotic cell death induced by anchorage-free/cell-matrix-disrupted conditions.[19,20] To achieve distant dissemination, cancer cells must overcome anoikis thought to be achieved by an increase in the expression of integrins compatible with the surrounding extracellular matrix (ECM), overexpression of pro-survival receptor tyrosine kinases that can compensate for missing integrins, cytoskeletal rearrangement for mechano-sensing or sustainability of an EMT phenotype.[21] Indeed, EMT induction via silencing E-cadherin[22] or sFRP1[23] can protect mammary epithelial cells against anoikis. These results indicate that the gain of a mesenchymal phenotype confers anoikis resistance, with possibly common regulators between these two systems.[21,24]

Ovarian carcinoma (OC) is a unique entity among cancers with EMT involvement.[25–27] Metastasis in OC is established by the EMT-driven delamination of OC cells from the primary tumour *in situ* and their penetration into the surrounding peritoneal cavity. EMT and its reversed process, mesenchymal–epithelial transition (MET), are frequently and actively involved in different phases of OC progression.[26] Although several EMT markers are correlated with clinical significance in OC,[27] a global clinical view of EMT and its potential intermediate state(s) has not been elucidated. In this study, we describe a model system for appraising the heterogeneous spectrum of EMT using a panel of well-characterised OC cell lines.[13,28] Our detailed phenotypic characterisation of their epithelial–mesenchymal compositions

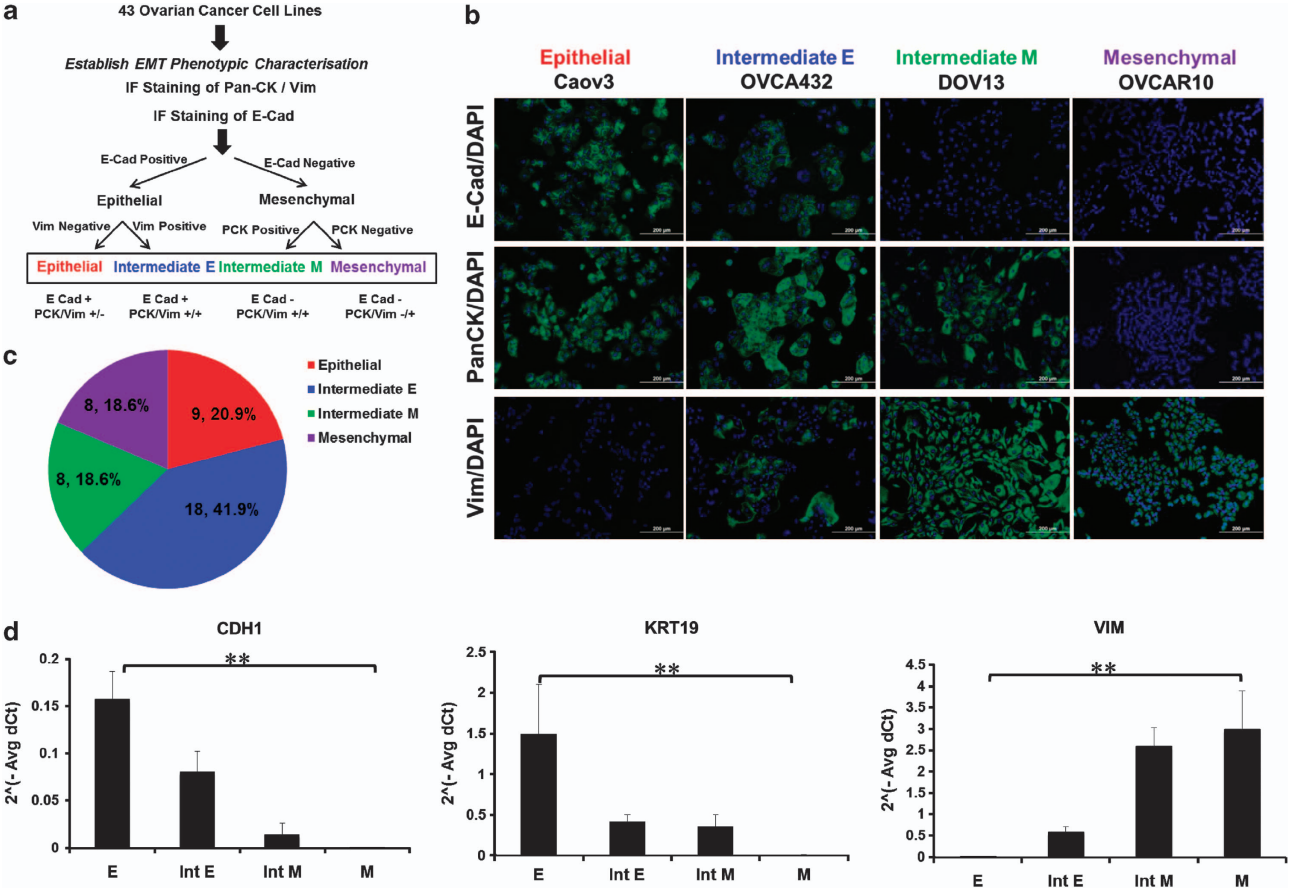

Figure 1 Identification of epithelial–mesenchymal phenotypes and EMT Spectrum in SGOCL(43). (**a**) The EMT phenotypic characterisation was achieved using IF staining of E-cadherin (E-cad), pan-cytokeratin (PCK) and Vimentin (Vim). Four phenotypes were identified: Epithelial (E-cad-positive, PCK-positive, Vim-negative), Intermediate E (E-cad-positive, PCK-positive, Vim-positive), Intermediate M (E-cad-negative, PCK-positive, Vim-positive) and Mesenchymal (E-cad-negative, PCK-negative, Vim-positive). (**b**) Phase contrast images (Phase) and IF staining of E-cadherin (E-cad), Pan-cytokeratin (PCK) and Vimentin (Vim) in Caov3, OVCA432, DOV13 and OVCAR10, representing Epithelial, Intermediate E, Intermediate M and Mesenchymal phenotypes, respectively. Scale bar = 200 μm. (**c**) Pie chart of the number and percentage distribution of four phenotypes in SGOCL(43). (**d**) Plot of QPCR expressions (2^- Avg ΔC_t) of the key EMT genes E-cadherin (*CDH1*), cytokeratin 19 (*KRT19*) and vimentin (*VIM*), showed a gradient along Epithelial (**e**), Intermediate E (Int E), Intermediate M (Int M) and Mesenchymal (M) phenotypes. Statistical significance at $^{**}P < 0.05$ in both ANOVA and Kruskal–Wallis test

describes an intermediate phenotype with both epithelial and mesenchymal characteristics that confers a more aggressive phenotype.

Results

Four phenotypic subgroups identified by epithelial–mesenchymal status. An OC library comprising 43 cell lines (SGOCL(43); Supplementary Table 1), was utilised to explore EMT heterogeneity. The epithelial–mesenchymal phenotype for each cell line was characterised by morphological examination and immunofluorescence (IF) staining for prototypic EMT markers. A decision flow was established to determine the phenotype of each line based on the IF pattern of E-cadherin, pan-cytokeratin and vimentin (Figure 1a; Materials and Methods). SGOCL(43) was characterised into four epithelial–mesenchymal phenotypes: Epithelial, Intermediate Epithelial (Intermediate E), Intermediate Mesenchymal (Intermediate M) and Mesenchymal (Figures 1a and b; Supplementary Table 2), with 9 (20.9%) Epithelial, 18 (41.9%) Intermediate E, 8 (18.6%) Intermediate M and 7 (18.6%) Mesenchymal (Figure 1c) phenotypes.

Establishing an EMT spectrum. To validate EMT gene expression among the four phenotypes, we utilised a commercially available quantitative PCR (QPCR) amplification array of 84 EMT-related genes. Of these, 34 genes showed significant differences in expression among the four EMT phenotypes (ANOVA or Kruskal–Wallis test; Table 1 and Supplementary Table 3), with significant differences observed for *CDH1*, *KRT19* and *VIM* expression. A gradient pattern was observed among the four phenotypes (Figure 1d) – for instance, *CDH1* and *VIM* displayed descending and ascending trends, respectively (Figure 1d and Table 1) – with a significant negative correlation (Spearman correlation coefficient: -0.66; *P*-value: 2.65411e-006). Thus, the phenotypic categorisation of SGOCL(43) created an EMT Spectrum within which EMT markers adhere to an EMT gradient. Several other EMT-related genes also demonstrated a gradient of expression, with *DSP*, *F11R* and *IL1RN* following the same descending trend as *CDH1* (Table 1) and *TWIST1* and *ZEB2* that of *VIM*. Interestingly, *CDH2*, which encodes N-cadherin, displayed an ascending trend that peaked at Intermediate M (Figure 2a and Table 1), as did other genes crucial for cell–microenvironment interactions – *ITGA5* and *MMP2* (Figure 2a). IF staining for N-cadherin in SGOCL(43) confirmed its cell-surface expression in 75% of the Intermediate M-classified lines (Figures 2b and c). Notably, $\sim$44.4% of Intermediate E lines, such as OVCA432, co-expressed both E- and N-cadherin at the cell surface (Figures 2b and c). Of particular interest, the expression of *ERBB3*, a member of the epidermal growth factor receptor family, was highest in Epithelial and Intermediate E cell lines and lowest in Intermediate M lines (Figure 2d), which was also confirmed using ELISA (Figure 2e).

EMT spectrum reveals a sequential expression pattern of classic EMT drivers. We next sought to ascertain the expression pattern of EMT drivers along the EMT Spectrum.

Table 1 Statistical significance of QPCR expression of EMT genes in SGOCL(43) EMT spectrum

Gene symbol	*P*-value (KW)	Expression pattern
CDH1	8.79E-06**	Descending
DSP	0.0004348**	Descending
F11R	0.0153598*	Descending
FGFBP1	0.0008591**	Descending
IL1RN	0.0007688**	Descending
JAG1	0.0133748*	Descending
KRT19	4.85E-05**	Descending
MST1R	0.0013871**	Descending
WNT11	0.0495988*	Descending
AKT1	0.0328503*	Nadir at Int E
WNT5A	0.0473454*	Nadir at Int E
ERBB3	0.000465**	Nadir at Int M
TWIST1	0.0019854**	Ascending
VIM	2.68E-05**	Ascending
WNT5B	0.0329648*	Ascending
ZEB2	0.0001512**	Ascending
GNG11	0.003524**	Peak at Int E
SNAI1	0.032298*	Peak at Int E
BMP7	0.0493499*	Peak at Int M
CDH2	0.0138235*	Peak at Int M
FN1	0.0193777*	Peak at Int M
ILK	0.0069188**	Peak at Int M
ITGA5	0.0019977**	Peak at Int M
MAP1B	0.0037885**	Peak at Int M
MMP2	0.0209024*	Peak at Int M
SERPINE1	0.0161845*	Peak at Int M
SOX10	0.0336869*	Peak at Int M
VCAN	0.0496592*	Peak at Int M
ZEB1	2.20E-05**	Peak at Int M
ESR1	0.0186407*	No pattern
MITF	0.0087447**	No Pattern
TGFB1	0.0382433*	No Pattern

*P-value <0.05; **P-value <0.01

FOXC2, *GSC* and *SNAI2* showed no significant difference in expression (Supplementary Table 3), whereas *SNAI1*, *TWIST1*, *ZEB1* and *ZEB2* showed sequential expression along the EMT Spectrum, with variable peaks in expression of *SNAI1* and *ZEB1* (Intermediate E) and *TWIST1* and *ZEB2* (Mesenchymal) (Figure 2f). Furthermore, *CDH2* and *ERBB3* at Intermediate M were apparently correlated with *ZEB1* expression (Figures 2a and d). These results suggest the existence of different waves of expression of EMT drivers along the EMT Spectrum.

Intermediate M phenotype has higher anoikis resistance and spheroid-forming ability *in vitro*. To explore the biological functions of these different phenotypes along the EMT Spectrum, several EMT-related functional analyses were performed on selected lines. OC aggressiveness is often marked by the presence of malignant ascites, where OC cells are shed and survive in suspension as single cells or spheroids once overcoming anoikis.[29] Thus, we compared the viability index (VI) of cells grown under conditions of ultra-low attachment suspension (ULAS) to those grown on normal tissue culture plastic (TCP). Generally, all four phenotypes survived well on TCP, (VI >1.0; Supplementary Figure 2), whereas in ULAS, the VI dropped significantly in most cell lines, indicating that the suspension was unfavourable for growth. However, for all Mesenchymal (100%) and the majority of Intermediate M (75%) lines, the VI was above

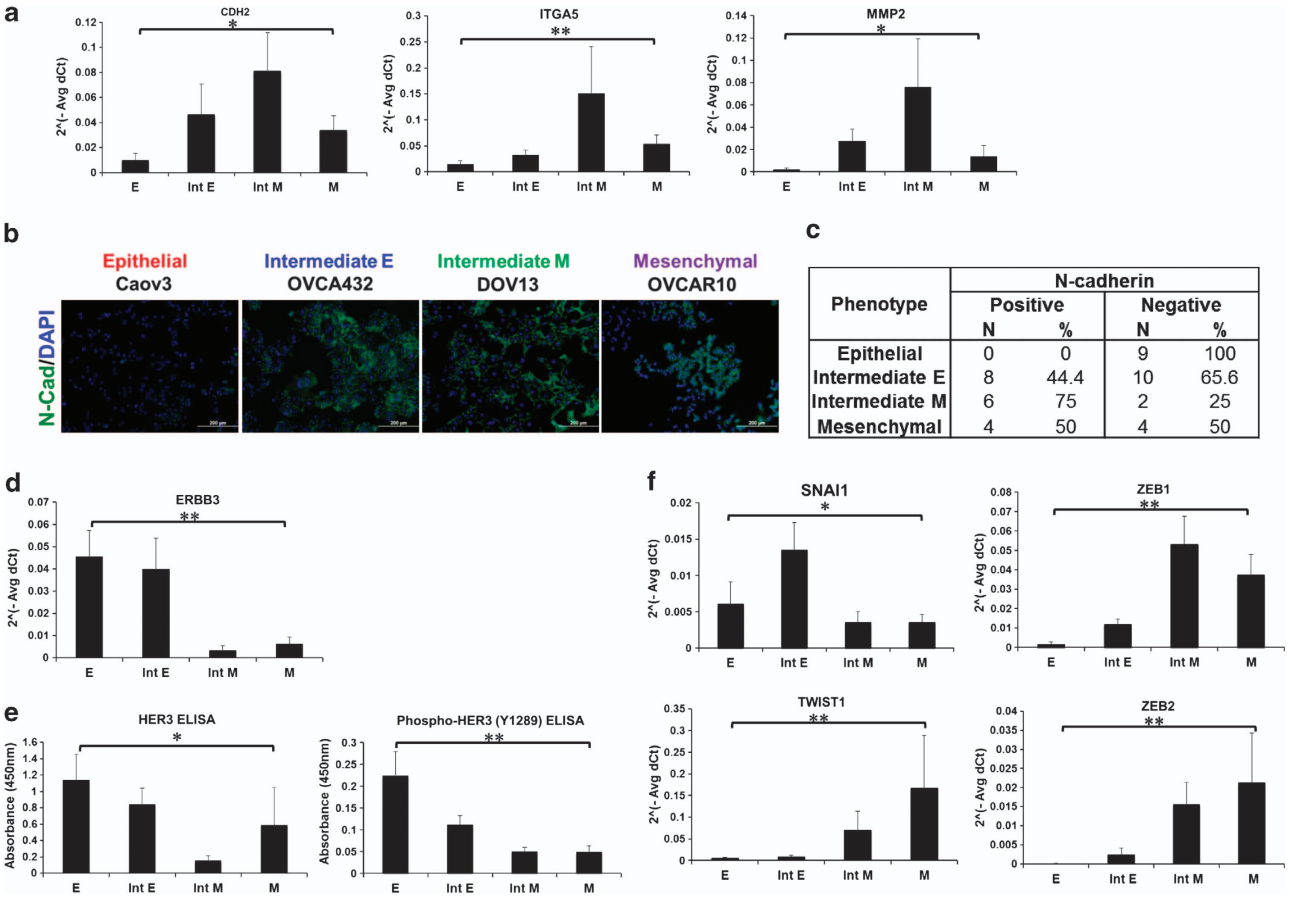

Figure 2 The Intermediate M phenotype is hallmarked by higher N-cadherin and ZEB1 and lower ERBB3 expressions. (**a**) Plot of QPCR expressions (2^- Avg ΔC_t) of *CDH2*, *ITGA5*, *MMP2* showing the peak expression at Intermediate M (Int M) phenotype. Statistical significance at $^{*}P<0.05$. (**b**) IF staining of N-cadherin (N-cad) in Caov3, OVCA432, DOV13 and OVCAR10 representing Epithelial, Intermediate E, Intermediate M and Mesenchymal phenotypes, respectively. Scale bar = 200 μm. (**c**) Distribution of N-cadherin IF positivity among four phenotypes in number (N) and percentage (%). (**d**) Plot of QPCR expressions (2^- Avg ΔC_t) of v-erb-b2 erythroblastic leukaemia viral oncogene homologue 3 (*ERBB3*) showed lowest expression in the Intermediate M phenotype. Statistical significance at $^{**}P<0.05$ at both ANOVA and Kruskal–Wallis test. (**e**) ELISA (**f**) Plot of QPCR expressions (2^- Avg ΔC_t) of snail homologue 1 (*SNAI1*), zinc-finger E-box-binding homeobox 1 (*ZEB1*), twist homologue 1 (*TWIST1*) and zinc-finger E-box-binding homeobox 2 (*ZEB2*) showing differential expression peaks in Intermediate E (Int E), Intermediate M (Int M) and Mesenchymal (M) phenotypes, respectively. Statistical significance at $^{**}P<0.05$ in both ANOVA and Kruskal–Wallis tests; Statistical significance at $^{*}P<0.05$ in either ANOVA or Kruskal–Wallis test

1.0 in ULAS. Very few Epithelial (33.3%) or Intermediate E (25%) lines had a VI above 1.0 (Figures 3a and b). These data indicate that Mesenchymal and Intermediate M phenotypes might be more resistant to anoikis. We also observed morphological differences after 96 h in ULAS cultures. The majority of the tested lines formed 'grape-like', irregularly shaped aggregates (marked as A; Figures 3c and d) in ULAS, whereas almost all Intermediate M lines formed smooth contoured spheroids (S). Only one Epithelial line, OV90, showed spheroid formation but with significantly lower efficiency than that in Intermediate M SKOV3 line, which showed high spheroidogenic efficiency (SKOV3 expanded from <10 spheroids to ~ 50 spheroids/1000 cells following sequential passages in ULAS; Figure 3e). Cell migration and invasion assays *in vitro* showed that Intermediate M cells had a tendency toward higher migratory and invasive potential than other cell lines (Supplementary Figures 3A–D), and using a subcutaneous xenograft model in nude mice, we showed that the SKOV3 line caused tumour formation after 5 weeks in the absence of Matrigel (Figure 3f and Supplementary Figure 3F). Collectively, we conclude that Intermediate M cells are more anoikis-resistant, display increased spheroidogenic potential and have a tendency toward increased migration and invasion. Thus, the Intermediate M phenotype might represent an aggressive category *in vitro*.

Relevance of EMT Spectrum in other cancers. To demonstrate the relevance of the EMT Spectrum in other cancers, we tested the lung adenocarcinoma cell line, A549, which exhibits an Intermediate E phenotype, as determined by its co-expression of E-cadherin, N-cadherin, cytokeratins and vimentin. Performing single clone selection, we isolated two clones exhibiting epithelial (A549E-A6) or mesenchymal (A549M-L3) morphology from the parental A549 (A549P) cells. A549E-A6 exhibited a rounded shape in sparse cultures and a cobblestone-like monolayer in confluent cultures, whereas A549M-L3 exhibited an elongated cell shape in sparse and confluent cultures (Figure 4a). From QPCR, we found that A549P expressed *CDH1* and *CDH2* at comparable levels, whereas A549E-A6 and A549M-L3 preferentially

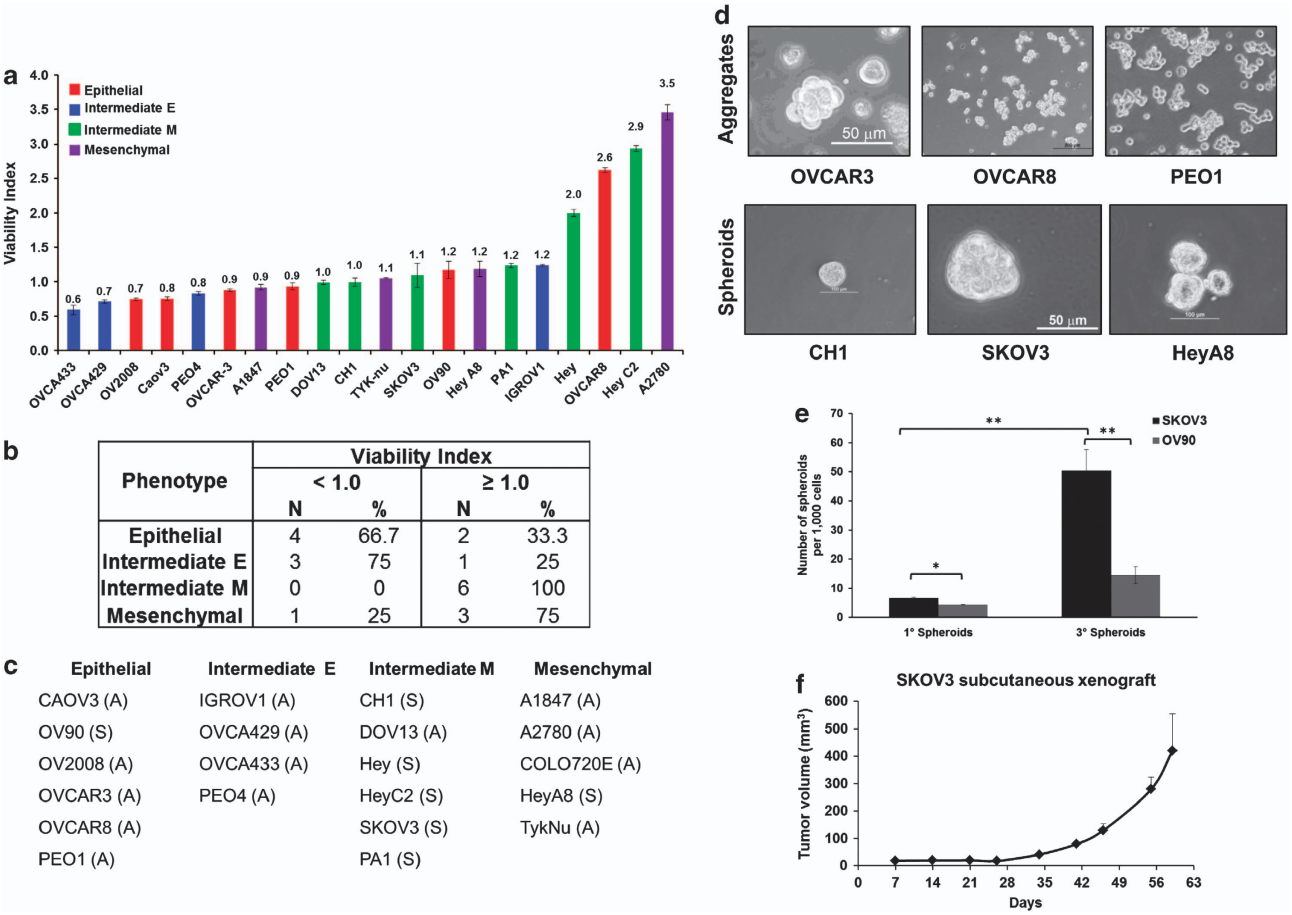

b

Phenotype	Viability Index			
	< 1.0		≥ 1.0	
	N	%	N	%
Epithelial	4	66.7	2	33.3
Intermediate E	3	75	1	25
Intermediate M	0	0	6	100
Mesenchymal	1	25	3	75

c

Epithelial	Intermediate E	Intermediate M	Mesenchymal
CAOV3 (A)	IGROV1 (A)	CH1 (S)	A1847 (A)
OV90 (S)	OVCA429 (A)	DOV13 (A)	A2780 (A)
OV2008 (A)	OVCA433 (A)	Hey (S)	COLO720E (A)
OVCAR3 (A)	PEO4 (A)	HeyC2 (S)	HeyA8 (S)
OVCAR8 (A)		SKOV3 (S)	TykNu (A)
PEO1 (A)		PA1 (S)	

Figure 3 Anoikis resistance, spheroid formation and tumour formation in selected cell lines of SGOCL(43). (**a**) Plot of viability index (*y* axis) measured by MTT absorbance ratio between 96 and 48 h in ultra-low attachment plates in Epithelial, Intermediate E, Intermediate M and Mesenchymal phenotypes. Error bars represented S.E.M. from triplicate cultures. (**b**) Distribution of viability index among four phenotypes in number (*N*) and percentage (%). (**c**) Summary of aggregate (A) or spheroid (S) formation in suspension cultures in selected cell lines from SGOCL(43). (**d**) Images of cell aggregates and spheroids in selected cell lines from SGOCL(43). (**e**) Plot of number of spheroid formed per 1000 cells (*y* axis) in SKOV3 and OV90 in primary (1^0) and tertiary (3^0) spheroid (*x* axis) cultures. Error bars represented S.E.M from triplicate cultures. Statistical significance at $^{**}P<0.01$.Statistical significance at $^{*}P<0.05$. (**f**) Growth curve of SKOV3 xenograft volume (*y* axis) in nude mice over time (*x* axis). Error bars represented S.D. from 6 subcutaneous engraftments in three mice

expressed *CDH1* and *CDH2*, respectively (Figure 4b and Supplementary Table 4). In addition, A549M-L3 showed a higher expression of *ZEB1* and lower *ERBB3* as compared with A549E-A6 and A549P (Figure 4b and Supplementary Table 4). Thus, the A549M-L3 clone may resemble an Intermediate M phenotype. In spheroid-forming assays, A549M-L3 displayed high spheroid-forming efficiency, whereas A549E-A6 only formed huge cell clumps in ULAS (Figures 4c and d). These data suggest that an Intermediate M-like sub-clone of A549 was more aggressive *in vitro* and that the phenomenon is not exclusive to OC.

Saracatinib (AZD0530) restores E-cadherin expression in intermediate M phenotype. Inhibitors targeting ALK5, MEK and Src kinases can induce EMT reversal.[30] We utilised these inhibitors to test whether we could alter the four EMT phenotypes. As compared with OVCAR3 (Epithelial), OVCA433 (Intermediate E) and OVCAR10 (Mesenchymal) cells, only SKOV3 (Intermediate M) cells underwent reversal after treatment with the Src-kinase inhibitor Saracatinib (AZD0530) (Figure 5a and Supplementary Figure 4). Furthermore, in AZD0530-treated SKOV3 cells, QPCR analysis showed a significant, dose-dependent upregulation in *CDH1* transcripts (Figure 5b, Supplementary Figure 5A), decreases in *SNAI1* and *SNAI2* (Supplementary Figure 4B) but no change in *ZEB1*, *ZEB2* or *TWIST1* (Supplementary Figure 4B). We also measured a fivefold increase in E-cadherin promoter activity in AZD0530-treated SKOV3 cells, with a concomitant increase in E-cadherin protein levels (Figures 5c and d). The AZD0530-treated SKOV3 tumour xenograft in mice also showed a dramatic increase in E-cadherin immunoreactivity (Figure 5e). These data demonstrate that the Intermediate M phenotype of SKOV3 cells could be reversed by inhibiting Src kinase.

Saracatinib (AZD0530) affects spheroid formation in intermediate M SKOV3 cells. We next tested whether AZD0530 would render the Intermediate M cells anoikis-sensitive and tested its effects on spheroid formation. As demonstrated above, VI in ULAS was significantly lower than cells on TCP with or without AZD0530. In addition, VI was significantly reduced with AZD0530 treatment in both

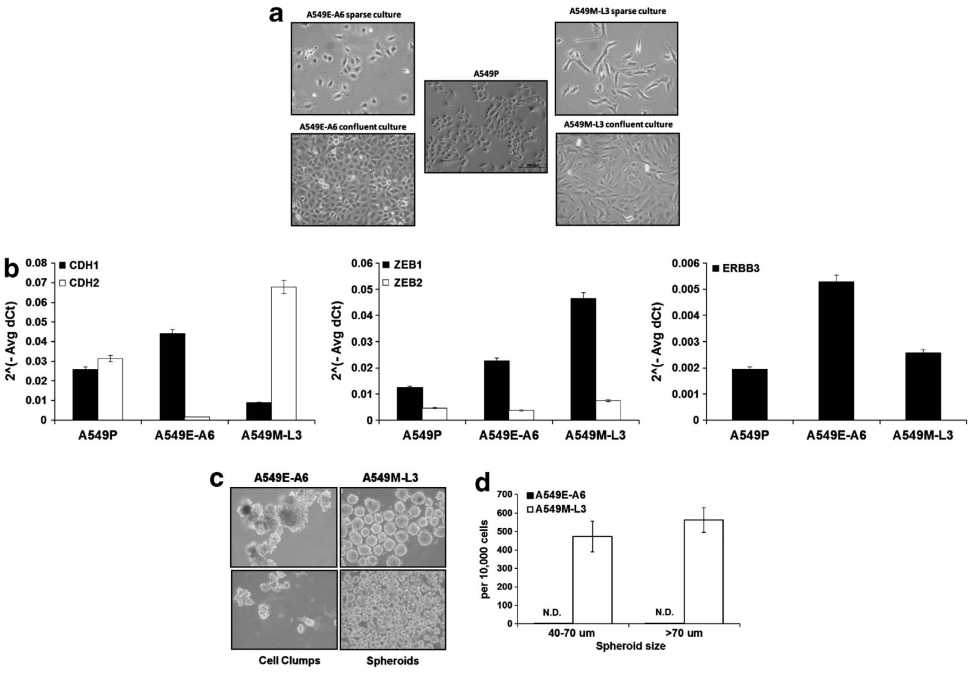

Figure 4 EMT heterogeneity in A549 cells. (**a**) Phase contrast images of two phenotypically distinct clones presenting epithelial (A549E-A6; left) and mesenchymal (A549M-L3; right) in sparse (upper) and confluent (lower) cultures compared with parental A549 cultures (A549P; centre). (**b**) Plot of QPCR expressions ($2^{\wedge}$- Avg ΔC_t) of *CDH1* and *CDH2* (left), *ZEB1* and *ZEB2* (middle), and *ERBB3* (right) in A549P, A549E-A6 and A549M-L3 cells. Error bars represented S.E.M. from triplicate cultures. (**c**) Images of spheroid formation in A549E-A6 (left) showing only cell clumps and in A549M-L3 (right) showing well-formed spheres. (**d**) Qualitative graph showing spheroid-forming numbers (*y* axis) in A549E-A6 and A549M-L3 cells. (N.D. indicates non-detectable). Error bars represented S.E.M. from triplicate cultures

conditions; however, the difference in VI was larger for cells on TCP (Figure 5f). This suggests that Src kinase may not have a major role in anoikis resistance. However, AZD0530 significantly decreased spheroid formation efficiency and average spheroid size in ULAS cultures (Figures 5g–i), although administering AZD0530 did not alter the size or weight of mice following SKOV3 xenograft (data not shown).

EMT signature identifies an Intermediate subgroup of OC patients with worse progression-free survival (PFS). To verify the clinical relevance of the intermediate EMT states identified *in vitro*, we utilised an EMT Signature to stratify OC patients based on different EMT states. Three genes, *CDH1*, *ZEB1*, and *ERBB3,* were used to generate gene expression signatures: *CDH1* represents the descending EMT gradient; *ZEB1*, the peak at Intermediate M; and *ERBB3*, the nadir at Intermediate M. A Venn diagram was then used to compare commonly encountered gene IDs that we believed represented the key components in EMT (Figure 6a). Table 2 shows the complete list of 36 probe-set IDs representing 33 identified genes.

Three genes overlapped with the genes that showed peak expression at Intermediate M in the EMT array: *ITGA5*, *VIM* and *ZEB1* (Figure 2a and Table 1). To further test how well their expression patterns fit with our IF-based classification scheme, we validated the selected genes from the EMT Signature that have been reported to be involve in EMT and not included in the initial EMT array (Table 2) in SGOCL (43). *PRSS8* and *RAB25* showed a gradient pattern similar to the EMT Spectrum (Supplementary Figure 7A), whereas *EPCAM*, *ESRP1* (Supplementary Figure 7B), *DDR1* and *GRHL2* (data not shown) expression levels were lowest at Intermediate M. This further confirmed the robustness of our IF-based EMT Spectrum and the validity of utilising the EMT Signature to stratify OC patients.

Hierarchical clustering of the expression profiles of an OC data set GSE9891[31] using the 33-gene EMT Signature identified four clusters: Epithelial (E), Intermediate E (IE), Intermediate M (IM) and Mesenchymal (M) (Figure 6b). From the PFS analysis, these four clusters showed interesting trends in PFS (Figure 6c). The 5-year PFS difference was significant in E *versus* M and IE *versus* M clusters (log-rank test; Figures 6c and d), with no other differences observed. We also found that the restricted mean survival time (RMST) difference at 60 months indicated a survival advantage of IE > E > IM > M (Figure 6e),[32] with only a slightly better PFS in the M cluster than in the IM (IM *versus* M: 2.185 at 60 months, Figure 6e; Supplementary Figure 7). Collectively, we conclude that the EMT Signature could be applied to identify a subcategory of OC tumours with an intermediate EMT status correlated with worse clinical outcome.

Discussion

The SGOCL(43) *in vitro* OC cell line model system was used to identify an EMT Spectrum. Only 20.9% of SGOCL(43) cell lines maintained the full epithelial phenotype, and 18.6% a full mesenchymal phenotype, with a complete loss of epithelial features. As such, most of the SGOCL(43) lines were in intermediate EMT states (60.5%), suggesting that most carcinoma cells gain mesenchymal features without completely losing their epithelial characteristics during EMT *in vitro*.

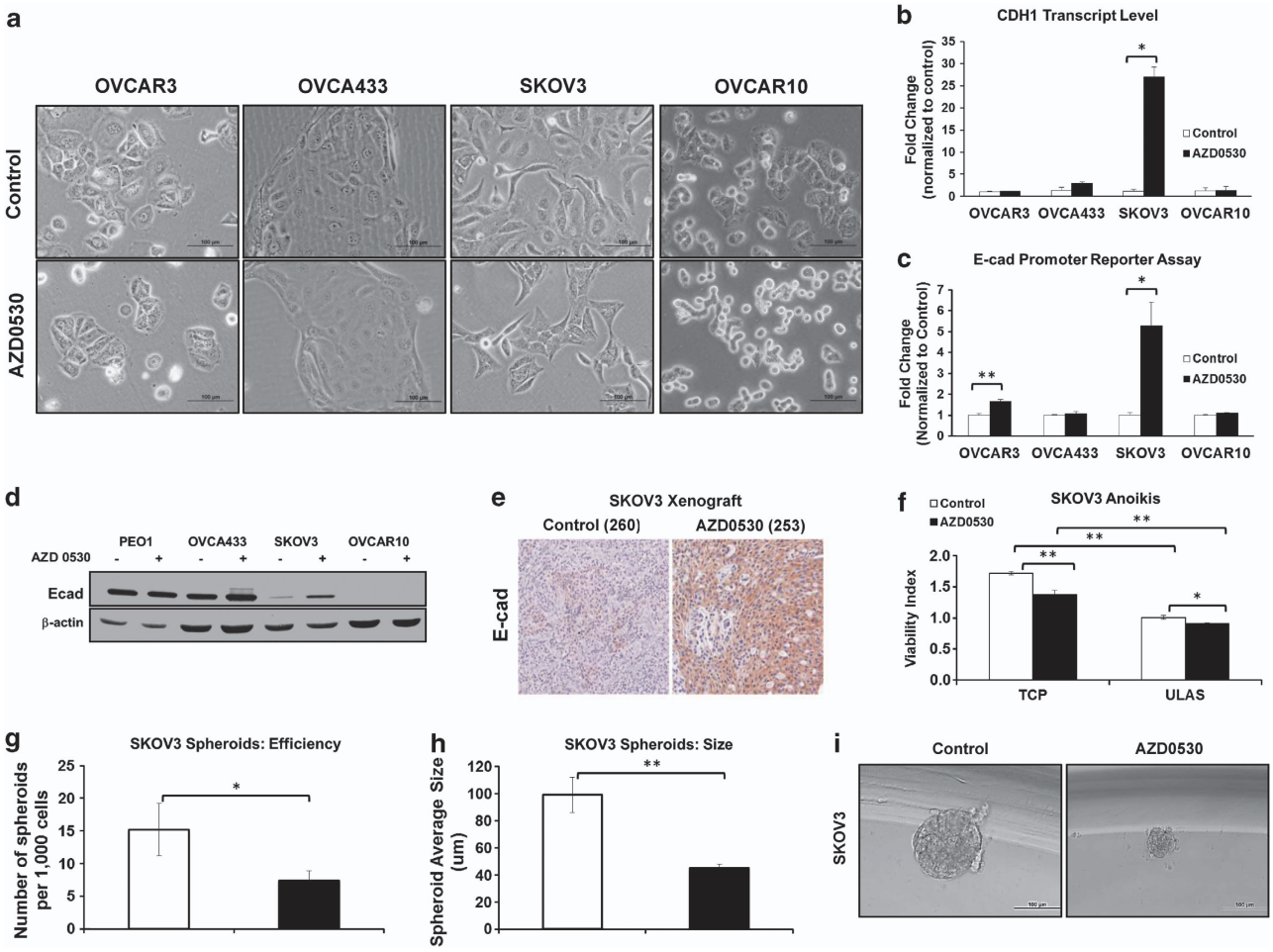

Figure 5 Reversibility of EMT and effects on anoikis resistance and spheroid formation by AZD0530 in Intermediate M SKOV3 cells. (**a**) Phase contrast images of OVCAR3, OVCA433, SKOV3 and OVCAR10 in control (upper panels)- or AZD0530 (lower panels)-treated cultures. Scale bar = 100 μm. (**b**) Plot of QPCR expression fold changes (*y* axis) of *CDH1* in control (blank box) or AZD0530 (solid box)-treated OVCAR3, -OVCA433, -SKOV3 and -OVCAR10 cells. (**c**) Plot of E-cadherin promoter activity fold changes (*y* axis) in control (blank box) or AZD0530 (solid box)-treated OVCAR3, -OVCA433, -SKOV3 and -OVCAR10 cells. (**d**) Western blots of E-cadherin (upper panel) and β-actin (lower panel) in control ($-$)- or AZD0530-treated ($+$) PEO1, -OVCA433, -SKOV3 and -OVCAR10 cells. (**e**) Representative images of immunohistochemistry staining of E-cadherin in control or AZD0530-treated SKOV3 xenografts. (**f**) Plot of viability index (*y* axis) of control (blank box) or AZD0530 (solid box)-treated SKOV3 cells in tissue culture plates (TCPs) and ULAS plates (*x* axis). (**g**) Plot of number of spheroid formed per 1000 cells (*y* axis) in control (blank box)- or AZD0530 (solid box)-treated SKOV3 cells. (**h**) Plot of average spheroid diameter (*y* axis) in control (blank box) or AZD0530 (solid box)-treated SKOV3 cells. (**i**) Images of spheroid formation in control or AZD0530-treated SKOV3 cells. Error bars represented S.E.M. from triplicate cultures. Statistical significance at $^{**}P<0.01$. Statistical significance at $^{*}P<0.05$

For example, A2780 cells stain negatively for E-cadherin but positively for N-cadherin at the junctions (Supplementary Figure 8), with weak cytoplasmic E-cadherin staining observed. As such, A2780 cells were categorised into the Mesenchymal subgroup, even though they display an 'epithelial'-like morphology. During the establishment or propagation of cell lines *in vitro*, clones that have undergone partial EMT within the heterogeneous population might already have more advantages during clonal selection as compared with cells that have not. As approximately two-thirds of the cell lines screened showed an intermediate phenotype, this suggests that a fully executed EMT might not be necessary for gaining growth advantages during clonal expansion. Indeed, others have shown that promotion of cell survival could be achieved via partial EMT.[33] Thus, the difference in the growth advantage for transitioned cells could explain the relatively limited cell lines with a solely Epithelial phenotype. However, the difference between Intermediate E and Intermediate M in resisting anoikis and forming spheroids suggests that a more complete EMT execution endows cells with increased aggressiveness.

During EMT, cells undergo a series of sequential events to disintegrate cell–cell contacts.[9] With the established EMT Spectrum, we were able to detect changes in gene expression patterns, with the sequential activation of major EMT drivers: for instance, *SNAI1* might be required early to downregulate *CDH1* followed by *ZEB1* to further accomplish the cadherin switch. These sequential changes support previous studies, where *SNAI1* is expressed at the onset of EMT and *SNAI2*, *ZEB1/2* and *TWIST* are induced later.[9,10,34] This EMT Spectrum will serve as a very informative tool, given that most of the current knowledge about EMT derives from binary separation between the epithelial and mesenchymal phenotypes.

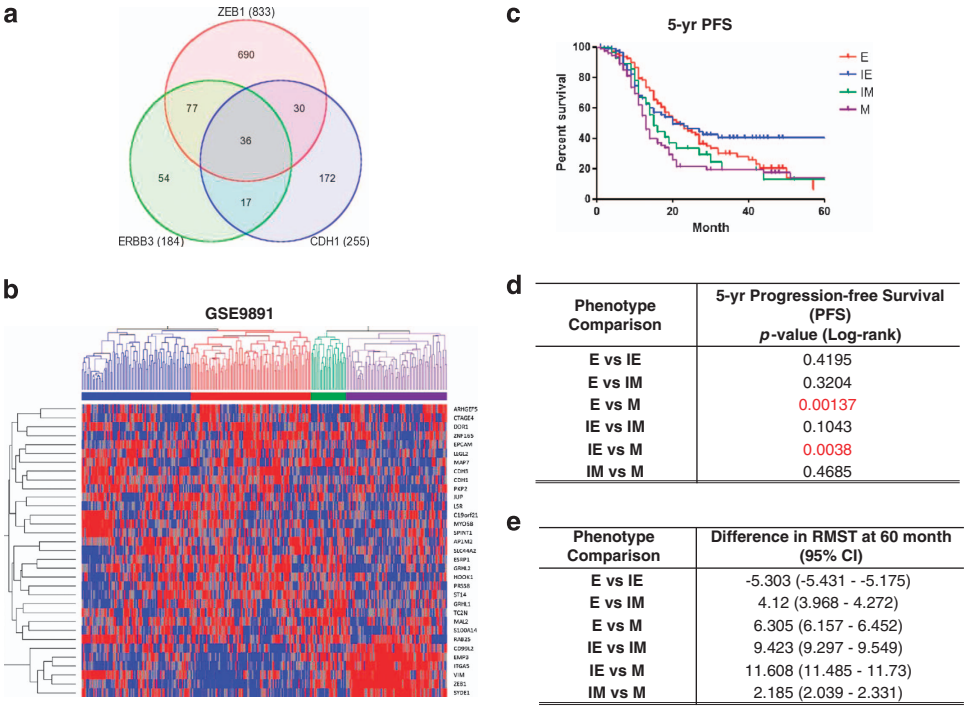

d

Phenotype Comparison	5-yr Progression-free Survival (PFS) *p*-value (Log-rank)
E vs IE	0.4195
E vs IM	0.3204
E vs M	0.00137
IE vs IM	0.1043
IE vs M	0.0038
IM vs M	0.4685

e

Phenotype Comparison	Difference in RMST at 60 month (95% CI)
E vs IE	-5.303 (-5.431 - -5.175)
E vs IM	4.12 (3.968 - 4.272)
E vs M	6.305 (6.157 - 6.452)
IE vs IM	9.423 (9.297 - 9.549)
IE vs M	11.608 (11.485 - 11.73)
IM vs M	2.185 (2.039 - 2.331)

Figure 6 EMT Signature identifies an Intermediate subgroup of ovarian carcinoma patients with shorter progression-free survival. (**a**) Venn diagram of *CDH1*, *ERBB3* and *ZEB1* signature showed 36 intersected common transcript IDs. (**b**) Hierarchical clustering of ovarian carcinoma collection GSE9891 using the 33-gene EMT Signature revealed four clusters Epithelial (red), Intermediate E (blue), Intermediate M (green) and Mesenchymal (purple). (**c**) Kaplan–Meier Survival plot for PFS at 5 years of GSE9891 collection separated into Epithelial (**e**), Intermediate E (Int E), Intermediate M (Int M) and Mesenchymal (M) clusters. (**d**) *P*-value summary of PFS analysis using log-rank test for paired comparison among four phenotypes. (**e**) Summary of PFS difference in RMST analysis for paired comparison among four phenotypes

Interestingly, despite the comparable anoikis resistance between Mesenchymal and Intermediate M phenotypes, the Mesenchymal cells lacked spheroid-forming ability in suspension cultures. This might be because of their decreased expression of genes important for cell–microenvironment interactions, such as *ITGA5* and *MMP2*. Interactions between $\alpha5\beta1$-integrin and fibronectin are reported to mediate OC spheroidogenesis and adhesion to ECM proteins at sites of secondary metastasis.[35] In the OC clinical data set, however, the PFS was similar between the Mesenchymal and Intermediate M groups. One plausible explanation is that clinical tumours designated as Mesenchymal are unlikely to be completely devoid of epithelial characteristics.[31] Therefore, these 'clinically' Mesenchymal tumours would resemble Intermediate M lines *in vitro*.

From our data, we also noticed that two Epithelial lines OVCAR8 and OV90 and one Intermediate E line IGROV1 demonstrated high VI in suspension cultures (Figure 3a). We previously showed that the IGROV1 cell line was molecularly characterised as 'Stem-A' as it demonstrated anchorage-independent growth in soft agar[13] and others have shown that OVCAR8 has spheroid-forming property in a hanging droplet method.[36] In the current study, OV90 also displayed spheroidogenic properties in ULAS cultures, albeit with limited efficiency (Figure 3e). These studies suggest that both the molecular properties and the EMT phenotype may contribute to anoikis resistance in OC cells and could explain why the three 'epithelial'-like cell lines showed high anoikis resistance in our study. Interestingly, IGROV1 and OVCAR8 did not form spheroids in ULAS as compared with the reported soft agar and hanging droplet systems,[13,36] perhaps suggesting that the ULAS culture condition is less favourable for these 'epithelial'-like cell lines to form spheroids despite their ability to overcome anoikis.

Two of three genes used to create the EMT Signature, *CDH1* and *ZEB1*, are well-characterised EMT factors.[1,10,37–39] *ERBB3*, on the other hand, has been less associated with EMT. *ERBB3*, which codes for the HER3 receptor, has a neuregulin-binding domain but not an active kinase domain. *ERBB3* is significantly increased in non-small cell lung cancer cell lines with an epithelial phenotype[16] and our data provide further support for the preferential expression of *ERBB3* in OC Epithelial cells. This is of special interest because the neuregulin/ERBB3 axis was recently shown to be a promising therapeutic target in OC.[36] Therefore, our findings illustrate that targeting *ERBB3/HER3* might only be effective in tumours that have not undergone EMT. Among the 33 genes in the EMT Signature, we noticed a higher frequency of epithelial over mesenchymal genes. This suggests that the threshold for losing epithelial characteristics during EMT might be lower than that for acquiring mesenchymal characteristics. This probably explains why the control of EMT is mainly via multiple negative regulatory loops,[10] such that lifting the suppression can allow the efficient execution of EMT. However, it is still intriguing whether these epithelial and mesenchymal genes are regulated by common or separate mechanisms. Among the 33 genes, 16 genes have been shown to be involved in EMT (Table 2),[3,40–58] whereas 17

Table 2 Summary of 33 key EMT component genes

Affy transcript ID	Symbol	Entrez gene name	Phenotype	Ref
8034084	*AP1M2*	Adaptor-related protein complex 1, mu 2 subunit	E	
8136987	*ARHGEF5*	Rho guanine nucleotide exchange factor (GEF) 5	E	40
8143610	*ARHGEF5*	Rho guanine nucleotide exchange factor (GEF) 5	E	40
8024013	*C19orf21*	Chromosome 19 open reading frame 21	E	
7996837	*CDH1*	Cadherin 1, type 1, E-cadherin (epithelial)	E	7
7996819	*CDH3*	Cadherin 3, type 1, P-cadherin (placental)	E	
8129560	*CTAGE6P*	CTAGE family, member 6, pseudogene	E	
8117900	*DDR1*	Discoidin domain receptor tyrosine kinase 1	E	49
8177867	*DDR1*	Discoidin domain receptor tyrosine kinase 1	E	49
8041853	*EPCAM*	Epithelial cell adhesion molecule	E	7,48,56
8098439	*EPCAM*	Epithelial cell adhesion molecule	E	7,48,56
8147351	*ESRP1*	Epithelial splicing regulatory protein 1	E	42,57,58
8040190	*GRHL1*	Grainyhead-like 1 (drosophila)	E	
8147697	*GRHL2*	Grainyhead-like 2 (drosophila)	E	43
7901765	*HOOK1*	Hook homologue 1 (drosophila)	E	
8015412	*JUP*	Junction plakoglobin	E	53
8009844	*LLGL2*	Lethal giant larvae homologue 2 (drosophila)	E	
8027793	*LSR*	Lipolysis stimulated lipoprotein receptor	E	
8148040	*MAL2*	mal, t-cell differentiation protein 2	E	44
8129783	*MAP7*	Microtubule-associated protein 7	E	
8023267	*MYO5B*	Myosin VB	E	
7962212	*PKP2*	Plakophilin 2	E	
8001007	*PRSS8*	protease, serine, 8	E	45
7906079	*RAB25*	RAB25, member RAS oncogene family	E	41
7920297	*S100A14*	S100 calcium binding protein A14	E	
8025672	*SLC44A2*	Solute carrier family 44, member 2	E	
7982829	*SPINT1*	Serine peptidase inhibitor, Kunitz type 1	E	46,47
7945204	*ST14*	Suppression of tumorigenicity 14 (colon carcinoma)	E	46,48
7980891	*TC2N*	Tandem C2 domains, nuclear	E	
8117630	*ZNF165*	Zinc-finger protein 165	E	
8175647	*CD99L2*	CD99 molecule-like 2	M	
8030007	*EMP3*	Epithelial membrane protein 3	M	
7963786	*ITGA5*	Integrin, alpha 5	M	50–52
8026407	*SYDE1*	Synapse defective 1, Rho GTPase, homologue 1 (C. elegans)	M	
7926368	*VIM*	Vimentin	M	7,55
7926916	*ZEB1*	Zinc-finger E-box binding homeobox 1	M	37,54

E, epithelial; M, mesenchymal

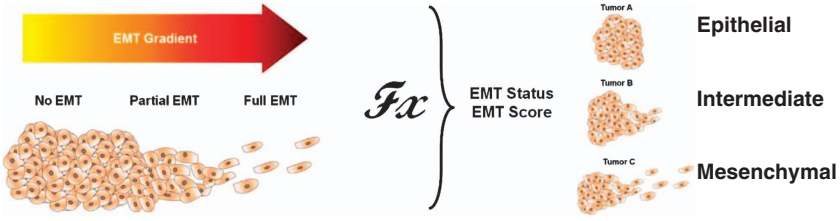

Figure 7 A proposed simplified scheme of EMT heterogeneity in carcinoma representing tumours harbouring a different EMT status as a function of undergoing various degrees of EMT process (No, Partial and Full EMT) under the cue of EMT gradient to acquire different phenotypes (Epithelial, Intermediate, and Mesenchymal)

genes have not. Gaining a further understanding of how these 17 EMT Signature genes are regulated and their functional role in EMT will be crucial in the quest for EMT-reversing agents. One possibility is that these EMT Signature genes can act as reporters for screening of EMT-reversing compounds. As AZD0530 had a differential effect on EMT Signature genes, with maximal effect on *CDH1*, it would be beneficial to find compounds that could also restore the expression of other epithelial genes for EMT reversal.

Finally, our subclassification of OC demonstrated that there might be intrinsic heterogeneity contributing to EMT in tumours. Our previous work, showing that the enrichment of EMT-related genes can define the Mesenchymal subtype, is very robust and reproducible.[13] Furthermore, the enrichment of EMT-related genes has been demonstrated in large OC data sets such as the Australian and TCGA OC cohorts.[59,60] Indeed, the Mesenchymal molecular subtype in the TCGA data set significantly correlated with this 33-gene EMT Signature. Using gene set enrichment analysis (GSEA), the Mesenchymal molecular subtype of the TCGA cohort was enriched in the Mesenchymal gene set ($P=0.046$) obtained from this EMT Signature (data not shown).

Phenotypic heterogeneity has been suggested in OC, as evidenced by subpopulations of transitory cells.[61] We propose that tumour heterogeneity can be summarised and represented as an EMT Status describing cells that undergo full,

partial or no EMT and leading to tumours with Epithelial, Intermediate or Mesenchymal phenotypes, respectively (Figure 7). EMT heterogeneity can be modelled by cell line characterisation to predict the *in vivo* tumour phenotype and outcome. Indeed, the reversal potential of the Intermediate M phenotype by AZD0530 may shed light on the potential clinical use of these compounds in EMT reversal; for instance, Intermediate M patients could be considered for trials of EMT-reversing agents postoperatively to better control PFS.

In conclusion, we identified an intermediate EMT phenotype with enhanced aggressiveness *in vitro*, characterised by high N-cadherin and ZEB1 expression and low E-cadherin and ERBB3/HER3 expression. An EMT Signature, derived from the molecular characterisation of this intermediate phenotype, can permit the subclassification of OC patients into four EMT States with differing clinical outcomes.

Materials and Methods

OC cell line library. An OC cell line library, termed SGOCL(43), consisting of 43 different OC cell lines of serous, endometrioid and undifferentiated histology, was acquired via various sources[28] and maintained in house. Detailed cell line names and growth conditions can be found in Supplementary Table 1. Supplementary Figure 1 shows the schematic presentation of the experimental design in establishing and characterising the ovarian cancer cell line library described in this study.

Immunofluorescence staining of EMT markers. Cells were grown on 15-mm glass coverslips (Paul Marienfeld GmbH & Co.KG, Germany) until 70–80% confluent. Cells were then fixed in cold acetone at $-20\,^{\circ}C$ for 10 min, rehydrated with $1\times$ PBS (thrice, 5 min each) and blocked with 3% (w/v) BSA (Fraction V, Sigma-Aldrich, St. Louis, MO, USA) in $1\times$ PBS for 1 h at room temperature. After washing with PBS, incubations with primary antibodies against E-cadherin (no. 610182, BD Biosciences, San Jose, CA, USA; 1:100), N-cadherin (no. M142, Takara Bio Inc, Shiga, Japan; 1:200), pan-cytokeratin (no. M3515, AE1/AE3, Dako, Denmark; 1:100) and vimentin (no. M7020, Dako; 1:100) were performed at $37\,^{\circ}C$ for 1 h. After washing with PBS, incubation with secondary antibodies conjugated with Alexa-488 (no. A11029, no. A11034, Invitrogen, Eugene, OR, USA) was performed at room temperature for 1 h in the dark. Slides were washed again with PBS, and coverslips were subsequently mounted onto the glass slides with anti-fading mounting media (Vector Laboratories Inc., Burlingame, CA, USA). All images were viewed on an Olympus IX71 fluorescent microscope and images were taken under $\times 10$ magnification using the Olympus DP71 camera (Olympus Optical Co. Ltd, Tokyo, Japan). The staining results were read by three independent researchers (JPT, SWJ and LYF). For E-cadherin and N-cadherin, only membranous junctional immunolabelling was regarded as positive (coded as 1 in Supplementary Table 2).

EMT phenotypic characterisation of SGOCL(43). E-cadherin immunoreactivity was utilised to determine the general epithelial (E-Cad-positive) or mesenchymal (E-Cad-negative) category. Subsequently, pan-cytokeratin and vimentin immunoreactivities were used to determine the differentiation subcategory. Cells assigned into the epithelial category that were also for vimentin immunoreactivity were designated as having a true epithelial (E) phenotype. Cells assigned into the mesenchymal category that were also negative for pan-cytokeratin immunoreactivity were designated as a true mesenchymal (M) phenotype. Cells that co-expressed pan-cytokeratin and vimentin were designated as Intermediates.

Nucleic acid isolation. RNA was isolated based on the protocols described in the miRNeasy Kit (no. 217004, Qiagen, GmbH, Germany). Briefly, cells were lysed in QIAzol reagent ($800\,\mu l/10\,cm^2$ culture surface area), and the lysate vigorously mixed with $160\,\mu l$ of chloroform before separating the aqueous phase via centrifugation ($12\,000\times g$, 15 min, $4\,^{\circ}C$). RNA was precipitated with $1.5\times$ volume of absolute ethanol (of aqueous phase) and purified using the spin columns provided in the kit. Isolated RNA was subsequently resuspended in nuclease-free water provided in the kit. RNA concentration was determined using the NanoDrop 1000 Spectrophotometer (Thermo Fisher Scientific, San Jose, CA, USA) and RNA integrity was analysed using the Agilent Bioanalyzer 2100 (Agilent, Santa Clara, CA, USA).

Protein extraction and western blotting. Protein was isolated on ice using cold RIPA buffer (no. R0278, Sigma-Aldrich) supplemented with protease (no. 539134) and phosphatase (no. 524625) inhibitor cocktails (Calbiochem, Boston, MA, USA). Protein concentration was quantitated using the BCA Protein Assay Kit (no. 23225, Thermo Fisher Scientific). SDS-PAGE electrophoresis was performed using 7.5% acrylamide gels that were transferred onto PVDF membranes (no. IPFL00010, Millipore, Billerica, MA, USA). Immunoblotting was performed by blocking the membranes with 5% skim milk (Nacalai Tesque, Kyoto, Japan) diluted in Tris-buffered saline (TBS), followed by incubating with mouse monoclonal anti-E-cadherin (no. 610182, BD Biosciences; 1:2500) or mouse monoclonal anti-β-actin (no. A1978, Sigma-Aldrich; 1:5000). Following washing steps, the membranes were then incubated with IRDye 800CW-conjugated goat anti-mouse (no. 926-32210) or IRDye 680-conjugated goat anti-mouse antibodies (no. 926-32220, LI-COR Biosciences, Lincoln, NE, USA). Following final washing steps, the western blots were scanned using an Odyssey Infrared Imaging System (LI-COR Biosciences).

Quantification of EMT status in carcinoma cell lines. SGOCL(43) cell lines were grown in 100-mm tissue culture plates (Corning Inc., Corning, NY, USA) until 90% confluence before harvesting. Each cell line was grown in duplicate. The RNA was extracted as described above using Qiazol (Qiagen) and prepared for real-time PCR using the miRNeasy columns (no. 217004, Qiagen). RNA (500 ng) was reverse transcribed into cDNA using the RT^2 First Stand Synthesis Kit (Qiagen, Germantown, MD, USA) and then subjected to real-time QPCR analysis of 84 known EMT pathway molecules (PAHS-090, Qiagen SABiosciences RT^2 Profiler EMT pathway). The reactions were carried out according to the manufacturer's protocol using the 7900HT Fast Real-Time PCR System (Applied Biosystems, Foster City, CA, USA) using the RT^2 qPCR SYBR/ ROX Master Mix and equal volumes of mixtures. Five housekeeping genes (HKGs) (*ACTB*, *B2M*, *GAPDH*, *HPRT1* and *RPL13A*) and five assay quality controls (one human genomic DNA contamination, two reverse transcription controls, two positive PCR control) were used as assay controls. Data in the form of threshold cycle numbers (C_t) were uploaded to the online data analysis portal (http://pcrdataanalysis.sabiosciences.com/pcr/arrayanalysis.php) to calculate the delta-C_t (ΔC_t). C_t was determined through the SDS (version 2.3) software (Applied Biosystems) by setting the baseline between cycle 2 of the run (total run: 40 cycles) and two cycles before the start of the first log-phase amplification. The threshold was set by positioning the limit to the lower one-third of the earliest amplification. ΔC_t was calculated by the respective formulae below:

$$\Delta C_t = C_t(\mathrm{GOI}) - C_t(\mathrm{HKG})$$

where by:

C_t (gene of interest, GOI): C_t value of the respective GOI,
C_t (HKG): average C_t values of the five HKGs used in the assay.

ELISA assay for HER3. Total protein lysates of SGOCL(43) ($25\,\mu g$) were subjected to enzyme-linked immunosorbent assay (ELISA) tests using PathScan Total HER3/ErbB3 Sandwich ELISA Kit (no. 7888) and PathScan Phospho HER3/ErbB3 (panTyr) Sandwich ELISA Kit (no. 7890 Cell Signalling Technology, Beverly, MA, USA). Phospho-HER3/ErbB3 (Tyr1289) (21D3) rabbit monoclonal antibody (no. 4791 Cell Signalling Technology) was used as the detection antibody replacing the panTyr antibody provided in the Phospho Kit. The absorbance at 450 nm wavelength was measured using TECAN Infinite 200 PRO microplate reader (Tecan, Crailsheim, Germany).

Anoikis assays and VI. Selected cell lines (CAOV3, OV90, OV2008, OVCAR3, OVCAR8, PEO1, IGROV1, OVCA429, OVCA433, PEO4, CH1, DOV13, Hey, HeyC2, SKOV3, A2780, A1847, HeyA88 and TYKNU) were used for the anoikis assay. Anoikis resistance assays were performed by seeding 1×10^5 cells into the wells of six-well plates of either normal tissue culture grade (TCP; no. 140675, Nunc, Denmark) or ultra-low attachment grade (ULA; no. 3471, Corning). Cells were incubated for 48 and 96 h prior to the MTT assay (no. G4100, Promega, Madison, WI, USA). Absorbance was read using a microplate reader (Tecan, Männedorf, Switzerland). The degree of anoikis resistance, termed VI,

was measured by the ratio of the absorbance readouts of MTT between 96 and 48 h. Anoikis resistance was determined if the VI measured above 1.0.

Spheroid assays and morphology examination. Cells of interest were trypsin-dissociated and strained through a 40-μm-pore strainer (no. 352340, BD Falcon, Franklin Lakes, NJ, USA). During quantification, the cell suspension was visually inspected for the presence of clumps using microscopy. Clumps were removed by additional rounds of straining until a single cell suspension was obtained. Single cells were seeded at a concentration of $\sim$18 cells/mm^2 ($\sim 10^5$ cells in a 100-mm dish, 55 cm^2 surface area) in ULA dishes (no. 3262, Corning Inc.). Cell suspension was incubated overnight with full media under standard conditions (37 °C, 5% CO_2) and strained as above after overnight to remove the presence of clumps. This was to prevent false-positive aggregates that may be mistaken for spheroids over prolonged culture. The cell suspension was incubated for a further period of 1–2 weeks for spheroid forming. Spheroids were determined by exhibiting a smooth surface of the compact multicellular masses by examining under a light microscope with proper phase contrast ring fitting (Nikon, Yokohama, Japan). Multicellular masses displaying uneven surface were determined as aggregates.

***In vivo* subcutaneous xenograft model.** The human OC cell lines, SKOV3, OVCAR3, OVCAR10 and OVCAR433, were maintained in complete high-glucose Dulbecco's modified Eagle's medium (DMEM), supplemented with 10% fetal bovine serum (FBS) and 1% penicillin and streptomycin; the cells were cultured at 37 °C in a humidified atmosphere containing 5% CO_2 and 95% air. The cells were harvested utilising 0.25% trypsin. Trypsin was inhibited using the same volume of complete medium. Cells were pelleted and resuspended in PBS in preparation for inoculation. All animal work adhered to the Agency of Science Technology and Research (A*STAR), Institutional Animal Care and use Committee (IACUC), guidelines on animal use and handling. Xenografts were generated by injecting 0.1 ml of 5×10^6 of each cell line subcutaneously into the dorsal flanks of female BALB/c nude mice (6–8 weeks old). Animal body weight and physical signs were monitored during the experiments. Tumour size was measured with vernier calliper every week. The tumour volume was calculated, with the formula: (length $\times$ width^2)/2.

***In vitro* EMT reversal assays.** Cells of interest were grown in complete media in either six-well plates (no. 140675, Nunc) or 100-mm dishes (no. 150350, Nunc) to allow growth until 60% confluence prior to drug treatment. DMSO control (no. D8418, Sigma-Aldrich; 0.05%) or AZD0530 at various concentrations were added for 24 h prior to downstream assays. Cells were examined under a light microscope with phase contrast rings (Olympus) to document morphological changes. RNA and protein were harvested and subjected to QPCR analysis and western blotting, respectively. For E-cadherin promoter assays, cells were seeded into 96-well plates (no. 3904, Corning Inc.) at a density of 0.5–1.0 $\times 10^4$ cells per well. After 24 h, the cells were transfected with E-cadherin promoter (a kind gift from Dr. Alice Wong, Hong Kong University) or vector control plasmid using XtremeGENE HP (no. 6366236001, Roche, Mannheim, Germany) with 2 : 1 HP : DNA ratio. The cells were treated with each drug on day 3 at a final concentration of 5 μM per well. The dual luciferase assay (no. E1960, Promega) was conducted on day 4 according to the manufacturer's protocol.

***In vitro* functional assays of AZD0530 treatment in SKOV3 cells.** SKOV-3 cells (ATCC, Manassas, VA, USA) were cultured in high-glucose DMEM (Nacalai Tesque) supplemented with 10% (v/v) FBS (Biowest SAS, Nuaillé, France). Cells were pretreated with either AZD0530 at 5 μM (final concentration) or a similar volume of DMSO (for control conditions, final concentration: 0.05% v/v) for 3 days prior to the respective assays. After the respective treatments, SKOV-3 cells were trypsin-dissociated, sorted using a 50-μm-mesh strainer and seeded at varying concentrations for the respective assays. During these assays, cells were treated as described before. For spheroid formation assays, pretreated SKOV-3 cells were seeded at a concentration of 200 cells/well onto a neutrally charged, ultra-low attachment surface (ULAS) 96-well plate (Corning Inc.) and treated as described above. Cells were incubated (2 weeks at 37 °C, 5% CO_2) and the spheroids that formed were visually counted using an inverted microscope (Olympus). For anoikis assays, pretreated SKOV-3 cells were seeded at a concentration of 1×10^5 cells/well in six-well plates and treated as per the conditions mentioned above. Each treatment was carried out on both Nunclon-Δ surface (Nunc) for adherent cultures or on neutral-charged ULAS for suspension culture. Cells were incubated for 48 and 96 h and an MTT assay (Promega) was carried out as per the instructions on the product user guide.

***In vivo* assays of AZD0530 treatment in SKOV3-luc-D3 cells.** All animal work adhered to the Agency of Science Technology and Research (A*STAR), IACUC guidelines on the use and handling of animals. SKOV3-Luc-D3 cells (Xenogen Co., Alameda, CA, USA) at a density of 3.5×10^6 in 100 μl of PBS were injected into the intraperitoneal cavity of 4-week-old female BALB/c nude mice. At 6 weeks post implantation, the mice were randomly divided into control and treatment groups ($n = 5$ animals per group). For the treatment group, mice were administered via oral gavage with 50 mg/kg AZD0530 (Selleck Chemicals, Houston, TX, USA) for 5 days a week for 2 weeks. The drug was re-suspended in 0.5% hydroxypropyl methylcellulose (Sigma-Aldrich) and 0.1% polysorbate buffer (Sigma-Aldrich). The control group received the vehicle buffer alone. The growth of tumour xenografts was monitored by bioluminescence using the IVIS system 2000 series (Xenogen Co.). The xenografts were harvested at 8 weeks post implantation for paraffin embedding followed by immunohistochemical staining for E-cadherin (no. 3195S; Cell Signalling Technology, Beverly, MA, USA).

Gene expression microarrays and generation of epithelial signatures. Affymetrix GeneChip Human Gene 1.0ST Array was used for gene expression analysis according to the protocols from the manufacturer. Data were pre-processed and RMA-normalised using Affymetrix Gene Expression Console. Expressions for genes were mean-aggregated for each gene based on Affymetrix probes annotation. Six cell lines with the highest expressions and six with the lowest expressions of *CDH1*, *ERBB3* and *ZEB1*, respectively, were selected to perform expression microarrays. The cell lines used in each signature is summarised below are as follows: CHD1 (High: Caov3, OVCA432, OVCA420, OAW42, OVCA433, C13; Low: Hey, TykNu, OVCAR10, A2780, BG1, HeyA8), ERBB3 (High: A1847, JHOS4, OVCA420, PEO1, OVCA429, OVCR8; Low: TykNu, HeyC2, OV7, OV56, HeyA8, SKOV3) and ZEB1 (High: OV7, TykNu, SKOV3, Hey, COLO720E, BG1; Low: OVCAR3, OV2008, A2008, C13, OVCAR8, JHOS4). *CDH1*, *ERBB3* and *ZEB1* signatures were generated by Partek Genomic Suites version 6.6 by using Student's *t*-test with FDR of 0.05.

EMT status identification in GSE9891and Kaplan–Meier survival analysis. To identify the EMT subtype in the GSE9891 cohort, unsupervised hierarchical clustering (correlation similarity metric; average-linkage) was performed independently on each cohort using the 33-gene signature. Robust Multi-array Average (RMA) was used for normalisation of the gene expression data. Genes with multiple probes were summarised into a single value by taking average gene expression. Prior input to unsupervised hierarchical clustering, the gene expression was standardised. EMT cluster assignment was derived from the branches of the hierarchical clustering tree and average gene expression of epithelial and mesenchymal gene clusters. For Kaplan–Meier analysis, the statistical significance was calculated by log-rank test from 277 samples with available clinical information. The RMST is estimated from the area under Kaplan–Meier curves using Matlab (r) R2012a trapezoidal area function, at $t = 12$, 24, 36, 48 and 60 months. The 95% confidence of RMST is estimated using t-distribution table.

Conflict of Interest

The authors declare no conflict of interest.

Acknowledgements. We thank the Biological Resource Centre at A*STAR for the animal work and histopathology facility at the Institute of Molecular and Cell Biology for the help in xenograft IHC. We thank Dr. R Jackson for her careful English editing. We are grateful for the financial support from the Cancer Science Institute of Singapore, Institute of Molecular Cellular Biology at A*STAR, National Medical Research Council/National University Cancer Institute Centre Grant: Pilot Grant FY2010, National University Health System Bench-to-Bedside Grant.

Author Contributions

RY-JH and JPT designed and conceived the study. RY-JH wrote the manuscript. MKW performed the cell line expansion experiments and, together with YFL and VYC, performed QPCR experiments. TZT and SM performed the microarray

analysis. HCL, JJL, MC provided clinical interpretation. NM provided some of the cell lines for SGOCL(43). RY-JH, MKW, YFL and EP performed the *in vitro* functional experiments. YFL, together with WJS, performed the immunofluorescence experiments and analysed the data. KTK, AHN and CT performed the AZD 0530 reversal experiments. YSC isolated the A549 clones.

1. Thiery JP. Epithelial-mesenchymal transitions in tumour progression. *Nat Rev Cancer* 2002; **2**: 442–454.
2. Thiery JP. Metastasis: alone or together? *Curr Biol* 2009; **19**: R1121–R1123.
3. Thiery JP, Sleeman JP. Complex networks orchestrate epithelial-mesenchymal transitions. *Nat Rev Mol Cell Biol* 2006; **7**: 131–142.
4. Kurrey NK, Jalgaonkar SP, Joglekar AV, Ghanate AD, Chaskar PD, Doiphode RY *et al.* Snail and slug mediate radioresistance and chemoresistance by antagonizing p53-mediated apoptosis and acquiring a stem-like phenotype in ovarian cancer cells. *Stem Cells* 2009; **27**: 2059–2068.
5. Kudo-Saito C, Shirako H, Takeuchi T, Kawakami Y. Cancer metastasis is accelerated through immunosuppression during Snail-induced EMT of cancer cells. *Cancer Cell* 2009; **15**: 195–206.
6. Mani SA, Guo W, Liao MJ, Eaton EN, Ayyanan A, Zhou AY *et al.* The epithelial-mesenchymal transition generates cells with properties of stem cells. *Cell* 2008; **133**: 704–715.
7. Guo W, Keckesova Z, Donaher JL, Shibue T, Tischler V, Reinhardt F *et al.* Slug and Sox9 cooperatively determine the mammary stem cell state. *Cell* 2012; **148**: 1015–1028.
8. Lee JM, Dedhar S, Kalluri R, Thompson EW. The epithelial-mesenchymal transition: new insights in signaling, development, and disease. *J Cell Biol* 2006; **172**: 973–981.
9. Huang RY, Guilford P, Thiery JP. Early events in cell adhesion and polarity during epithelial-mesenchymal transition. *J Cell Sci* 2012; **125**: 4417–4422.
10. Thiery JP, Acloque H, Huang RY, Nieto MA. Epithelial-mesenchymal transitions in development and disease. *Cell* 2009; **139**: 871–890.
11. Shoemaker RH. The NCI60 human tumour cell line anticancer drug screen. *Nat Rev Cancer* 2006; **6**: 813–823.
12. Neve RM, Chin K, Fridlyand J, Yeh J, Baehner FL, Fevr T *et al.* A collection of breast cancer cell lines for the study of functionally distinct cancer subtypes. *Cancer Cell* 2006; **10**: 515–527.
13. Tan TZ, Miow QH, Huang RY, Wong MK, Ye J, Lau JA *et al.* Functional genomics identifies five distinct molecular subtypes with clinical relevance and pathways for growth control in epithelial ovarian cancer. *EMBO Mol Med* 2013; **5**: 983–998.
14. Hanahan D, Weinberg RA. Hallmarks of cancer: the next generation. *Cell* 2011; **144**: 646–674.
15. Moreno-Bueno G, Peinado H, Molina P, Olmeda D, Cubillo E, Santos V *et al.* The morphological and molecular features of the epithelial-to-mesenchymal transition. *Nat Protoc* 2009; **4**: 1591–1613.
16. Thomson S, Buck E, Petti F, Griffin G, Brown E, Ramnarine N *et al.* Epithelial to mesenchymal transition is a determinant of sensitivity of non-small-cell lung carcinoma cell lines and xenografts to epidermal growth factor receptor inhibition. *Cancer Res* 2005; **65**: 9455–9462.
17. Buck E, Eyzaguirre A, Barr S, Thompson S, Sennello R, Young D *et al.* Loss of homotypic cell adhesion by epithelial-mesenchymal transition or mutation limits sensitivity to epidermal growth factor receptor inhibition. *Mol Cancer Ther* 2007; **6**: 532–541.
18. Huang RY, Wang SM, Hsieh CY, Wu JC. Lysophosphatidic acid induces ovarian cancer cell dispersal by activating Fyn kinase associated with p120-catenin. *Int J Cancer* 2008; **123**: 801–809.
19. Meredith JE Jr, Fazeli B, Schwartz MA. The extracellular matrix as a cell survival factor. *Mol Biol Cells* 1993; **4**: 953–961.
20. Frisch SM, Francis H. Disruption of epithelial cell-matrix interactions induces apoptosis. *J Cell Biol* 1994; **124**: 619–626.
21. Guadamillas MC, Cerezo A, del Pozo MA. Overcoming anoikis- pathways to anchorage-independent growth in cancer. *J Cell Sci* 2011; **124**: 3189–3197.
22. Onder TT, G PB, Mani SA, Yang J, Lander ES, Weinberg RA. Loss of E-cahderin promotes metastasis via multiple downstream transcriptional pathways. *Cancer Res* 2008; **68**: 3645–3654.
23. Gauger KJ, H JM, T MA, Schneider SS. Down-regulation of sfrp1 in a mammary epithelial cell line promotes the development of a cd44high/cd24low population which is invasive and resistant to anoikis. *Cancer Cell Ints* 2009; **9**: 11.
24. Frisch SM, S M, Cieply B. Mechanisms that link the oncogenic epithelial-mesenchymal transition to suppression of anoikis. *J Cell Sci* 2013; **126**: 21–29.
25. Chua KN, Poon KL, Lim J, Sim WJ, Huang RY, Thiery JP. Target cell movement in tumor and cardiovascular diseases based on the epithelial-mesenchymal transition concept. *Adv Drug Deliv Rev* 2011; **63**: 558–567.
26. Ahmed N, Abubaker K, Findlay J, Quinn M. Epithelial mesenchymal transition and cancer stem cell-like phenotypes facilitate chemoresistance in recurrent ovarian cancer. *Curr Cancer Drug Targets* 2010; **10**: 268–278.
27. Davidson B, Trope CG, Reich R. Epithelial-mesenchymal transition in ovarian carcinoma. *Front Oncol* 2012; **2**: 33.
28. Matsumura N, Huang Z, Mori S, Baba T, Fujii S, Konishi I *et al.* Epigenetic suppression of the TGF-beta pathway revealed by transcriptome profiling in ovarian cancer. *Genome Res* 2011; **21**: 74–82.
29. Ahmed N, Thompson EW, Quinn MA. Epithelial-mesenchymal interconversions in normal ovarian surface epithelium and ovarian carcinomas: an exception to the norm. *J Cell Physiol* 2007; **213**: 581–588.
30. Chua KN, Sim WJ, Racine V, Lee SY, Goh BC, Thiery JP. A cell-based small molecule screening method for identifying inhibitors of epithelial-mesenchymal transition in carcinoma. *PLoS One* 2012; **7**: e33183.
31. Tothill RW, Tinker AV, George J, Brown R, Fox SB, Lade S *et al.* Novel molecular subtypes of serous and endometrioid ovarian cancer linked to clinical outcome. *Clin Cancer Res* 2008; **14**: 5198–5208.
32. Royston P, Parmar MK. The use of restricted mean survival time to estimate the treatment effect in randomized clinical trials when the proportional hazards assumption is in doubt. *Stat Med* 2011; **30**: 2409–2421.
33. Leroy P, Mostov KE. Slug is required for cell survival during partial epithelial-mesenchymal transition of HGF-induced tubulogenesis. *Mol Biol Cell* 2007; **18**: 1943–1952.
34. Peinado H, Olmeda D, Cano A. Snail Zeb and bHLH factors in tumour progression: an alliance against the epithelial phenotype? *Nat Rev Cancer* 2007; **7**: 415–428.
35. Casey RC, Burleson KM, Skubitz KM, Pambuccian SE, Oegema TR Jr., Ruff LE *et al.* Beta 1-integrins regulate the formation and adhesion of ovarian carcinoma multicellular spheroids. *Am J Pathol* 2001; **159**: 2071–2080.
36. Sheng Q, Liu X, Fleming E, Yuan K, Piao H, Chen J *et al.* An activated ErbB3/NRG1 autocrine loop supports in vivo proliferation in ovarian cancer cells. *Cancer Cell* 2010; **17**: 298–310.
37. Schmalhofer O, Brabletz S, Brabletz T. E-cadherin beta-catenin, and ZEB1 in malignant progression of cancer. *Cancer Metastasis Rev* 2009; **28**: 151–166.
38. Sanchez-Tillo E, Lazaro A, Torrent R, Cuatrecasas M, Vaquero EC, Castells A *et al.* ZEB1 represses E-cadherin and induces an EMT by recruiting the SWI/SNF chromatin-remodeling protein BRG1. *Oncogene* 2010; **29**: 3490–3500.
39. Gregory PA, Bert AG, Paterson EL, Barry SC, Tsykin A, Farshid G *et al.* The miR-200 family and miR-205 regulate epithelial to mesenchymal transition by targeting ZEB1 and SIP1. *Nat Cell Biol* 2008; **10**: 593–601.
40. Mihira H, Suzuki HI, Akatsu Y, Yoshimatsu Y, Igarashi T, Miyazono K *et al.* TGF-beta-induced mesenchymal transition of MS-1 endothelial cells requires Smad-dependent cooperative activation of Rho signals and MRTF-A. *J Biochem* 2012; **151**: 145–156.
41. Vuoriluoto K, Haugen H, Kiviluoto S, Mpindi JP, Nevo J, Gjerdrum C *et al.* Vimentin regulates EMT induction by Slug and oncogenic H-Ras and migration by governing Axl expression in breast cancer. *Oncogene* 2011; **30**: 1436–1448.
42. Warzecha CC, Sato TK, Nabet B, Hogenesch JB, Carstens RP. ESRP1 and ESRP2 are epithelial cell-type-specific regulators of FGFR2 splicing. *Mol Cell* 2009; **33**: 591–601.
43. Cieply B, Riley P, Pifer PM, Widmeyer J, Addison JB, Ivanov AV *et al.* Suppression of the epithelial-mesenchymal transition by Grainyhead-like-2. *Cancer Res* 2012; **72**: 2440–2453.
44. Arumugam T, Ramachandran V, Fournier KF, Wang H, Marquis L, Abbruzzese JL *et al.* Epithelial to mesenchymal transition contributes to drug resistance in pancreatic cancer. *Cancer Res* 2009; **69**: 5820–5828.
45. Chen LM, Verity NJ, Chai KX. Loss of prostasin (PRSS8) in human bladder transitional cell carcinoma cell lines is associated with epithelial-mesenchymal transition (EMT). *BMC Cancer* 2009; **9**: 377.
46. Cheng H, Fukushima T, Takahashi N, Tanaka H, Kataoka H. Hepatocyte growth factor activator inhibitor type 1 regulates epithelial to mesenchymal transition through membrane-bound serine proteinases. *Cancer Res* 2009; **69**: 1828–1835.
47. Leshem O, Madar S, Kogan-Sakin I, Kamer I, Goldstein I, Brosh R *et al.* TMPRSS2/ERG promotes epithelial to mesenchymal transition through the ZEB1/ZEB2 axis in a prostate cancer model. *PLoS One* 2011; **6**: e21650.
48. Gemmill RM, Roche J, Potiron VA, Nasarre P, Mitas M, Coldren CD *et al.* ZEB1-responsive genes in non-small cell lung cancer. *Cancer Lett* 2011; **300**: 66–78.
49. Maeyama M, Koga H, Selvendiran K, Yanagimoto C, Hanada S, Taniguchi E *et al.* Switching in discoid domain receptor expressions in SLUG-induced epithelial-mesenchymal transition. *Cancer* 2008; **113**: 2823–2831.
50. White LR, Blanchette JB, Ren L, Awn A, Trpkov K, Muruve DA. The characterization of alpha5-integrin expression on tubular epithelium during renal injury. *Am J Physiol Renal Physiol* 2007; **292**: F567–F576.
51. Maschler S, Wirl G, Spring H, Bredow DV, Sordat I, Beug H *et al.* Tumor cell invasiveness correlates with changes in integrin expression and localization. *Oncogene* 2005; **24**: 2032–2041.
52. Nam EH, Lee Y, Park YK, Lee JW, Kim S. ZEB2 upregulates integrin alpha5 expression through cooperation with Sp1 to induce invasion during epithelial-mesenchymal transition of human cancer cells. *Carcinogenesis* 2012; **33**: 563–571.
53. Boyer B, Tucker GC, Valles AM, Gavrilovic J, Thiery JP. Reversible transition towards a fibroblastic phenotype in a rat carcinoma cell line. *Int J Cancer Suppl* 1989; **4**: 69–75.
54. Brabletz S, Brabletz T. The ZEB/miR-200 feedback loop–a motor of cellular plasticity in development and cancer? *EMBO Rep* 2010; **11**: 670–677.

55. Kokkinos MI, Wafai R, Wong MK, Newgreen DF, Thompson EW, Waltham M. Vimentin and epithelial-mesenchymal transition in human breast cancer–observations *in vitro* and *in vivo*. *Cells Tissues Organs* 2007; **185**: 191–203.
56. Evseenko D, Zhu Y, Schenke-Layland K, Kuo J, Latour B, Ge S *et al.* Mapping the first stages of mesoderm commitment during differentiation of human embryonic stem cells. *Proc Natl Acad Sci USA* 2010; **107**: 13742–13747.
57. Warzecha CC, Jiang P, Amirikian K, Dittmar KA, Lu H, Shen S *et al.* An ESRP-regulated splicing programme is abrogated during the epithelial-mesenchymal transition. *Embo J* 2010; **29**: 3286–3300.
58. Warzecha CC, Carstens RP. Complex changes in alternative pre-mRNA splicing play a central role in the epithelial-to-mesenchymal transition (EMT). *Semin Cancer Biol* 2012; **22**: 417–427.
59. Tothill RW, Tinker AV, George J, Brown R, Fox SB, Lade S *et al.* Novel molecular subtypes of serous and endometrioid ovarian cancer linked to clinical outcome 2008; **14**: 5198–5208.
60. Network TCGAR. Integrated genomic analyses of ovarian carcinoma. *Nature* 2011; **474**: 609–615.
61. Strauss R, Li ZY, Liu Y, Beyer I, Persson J, Sova P *et al.* Analysis of epithelial and mesenchymal markers in ovarian cancer reveals phenotypic heterogeneity and plasticity. *PLoS One* 2011; **6**: e16186.

Supplementary Information accompanies this paper on Cell Death and Disease website (http://www.nature.com/cddis)